

1 **A refinement of coccolith separation methods: Measuring the sinking**
2 **characters of coccoliths**

3 Hongrui Zhang^{1, 2}, Heather Stoll², Clara Bolton³, Xiaobo Jin¹, Chuanlian Liu¹

4 ¹ State Key Laboratory of Marine Geology, Tongji University, Shanghai, 200092, China

5 ² Geological Institute, Department of Earth Science, Sonneggstrasse 5, ETH, 8092, Zürich, Switzerland

6 ³ Aix-Marseille Univ, CNRS, IRD, Coll de France, CEREGE, Aix en Provence, France.

7 *Correspondence to:* Chuanlian Liu (liucl@tongji.edu.cn)

8 **Abstract.** Quantification sinking velocities of individual coccoliths will contribute to optimizing
9 laboratory methods for separating coccoliths of different sizes and species for geochemical analysis.
10 The repeat settling/decanting method was the earliest method proposed to separate coccoliths from
11 sediments, and is still widely used. However, in the absence of estimates of settling velocity for non-
12 spherical coccoliths, previous implementations have depended mainly on time consuming empirical
13 method development by trial and error. In this study, the sinking velocities of coccoliths belonging
14 to different species were carefully measured in a series of settling experiments for the first time.
15 Settling velocities of modern coccoliths range from 0.154 to 10.67 cm h⁻¹. We found that a quadratic
16 relationship between coccolith length and sinking velocity fits well and coccolith sinking velocity
17 can be estimated by measuring the coccolith length and using the length-velocity factor, k_v . We
18 found a negligible difference in sinking velocities measured in different vessels. However, an
19 appropriate choice of vessel must be made to avoid ‘hindered settling’ in coccolith separations. The
20 experimental data and theoretical calculations presented here support and improve the repeat
21 settling/decanting method.

22 **1. Introduction**

23 Coccolithophores are some of the most important phytoplankton in the ocean. They can secrete
24 calcareous plates called coccoliths, which contribute significantly to discrete particulate inorganic
25 carbon in the euphotic zone and to CaCO₃ fluxes to the deep ocean (e.g., Young and Ziveri, 2000;
26 Sprengel et al., 2002). Coccolith morphology, geochemistry and fossil assemblage composition
27 can reflect paleoenvironmental changes (e.g., Beaufort et al., 1997; Stoll et al., 2002; Zhang et al.,
28 2016). However, the use of coccolith geochemical analyses in paleoenvironmental reconstructions
29 was so far hindered by the difficulty of isolating coccolith compared with foraminifera. Two main
30 methods have been developed to concentrate near-monospecific assemblages of coccoliths from
31 bulk sediments: one is the method based on a decanting technique (Paull and Thierstein, 1987; Stoll
32 and Ziveri, 2002) and the other is that based on microfiltration (Minoletti et al., 2009). The
33 improvement of separation techniques offered a new perspective to study the Earth's history (e.g.
34 Stoll, 2005; Beltran et al., 2007; Bolton and Stoll, 2013; Rousselle et al., 2013). Moreover, the
35 development of coccolith oxygen and carbon isotope studies in culture in recent years (e.g. Ziveri
36 et al., 2003; Rickaby et al., 2010; Hermoso et al., 2016; McClelland et al., 2017) has provided an
37 improved mechanistic understanding of coccolith isotope data and therefore stimulated the need for
38 more purified coccolith fraction samples from the fossil record.

39 Both decanting and microfiltering are widely used methods for coccolith separation. The
40 microfiltering method separates coccoliths with polycarbonate micro-filter membrane (with pore
41 sizes of 2µm, 3µm, 5µm 8µm, 10µm and 12µm). This method is highly effective in the larger size
42 ranges, but is very time consuming in sediments with a high proportion of small (<5µm) coccoliths
43 (which tends to be the case in natural populations). It is also impossible to separate coccoliths with
44 similar lengths by microfiltration, such as *Florisphaera profunda* and *Emiliana huxleyi* (Hermoso
45 et al., 2015). Decanting, on the other hand, is highly effective for the small-sized coccoliths, because
46 their slow settling times permit a greater ability to separate different sizes. Consequently, in some
47 studies, a combination of the micro filtering and sinking or centrifugation method were applied for
48 coccolith separation (Stoll, 2005; Bolton et al., 2012; Hermoso et al., 2015). The repeated
49 sinking/decanting method, first employed by (Edwards, 1963; Paull and Thierstein, 1987) follows
50 the simple principle formalized by Stokes' Law for spherical particles: particles of larger size settle

51 more quickly because they have a higher ratio of volume and mass (accelerating sinking) to sectional
52 area (resistance retarding sinking). However, the sinking velocities of coccoliths with complex
53 shape are difficult to calculate and have not been quantified in previous studies. Consequently, the
54 repeated decanting method has generally used settling times based on empirical trial and error.
55 In the current study, we present a novel and rigorous estimation of sinking velocity for 16 species
56 of modern and Cenozoic coccoliths, carefully measured in 0.2% ammonia at 20°C. With this new
57 dataset, we explore how to estimate the sinking velocity of coccoliths based on their shape and
58 length, which allows our estimations to be generalized for other species, and for situations where
59 the mean length of coccoliths of a given species was different from that of our study. These
60 generalizations, together with our results on sinking velocities of one coccolith species
61 (*Gephyrocapsa oceanica*) in different vessels, should allow a significant improvement in efficiency
62 of future protocols for separation of coccoliths by repeated decanting.

63 **2. Materials and methods**

64 **2.1 Sample selections**

65 We measured the sinking velocity of 16 different species of coccoliths, isolated from eight deep-sea
66 sediment samples from the Pacific and Atlantic Oceans (Figure 1, Table A1). Sample were
67 principally of Quaternary age but include two Neogene/Paleogene samples. In general, numbers of
68 small coccoliths, including *E. huxleyi*, *Gephyrocapsa* spp and *Reticulofenestra* spp. are about an
69 order of magnitude greater than that of larger coccoliths. However, the larger coccoliths'
70 contributions to carbonate can be as high as 50% (Baumann, 2004; Jin et al., 2016). Moreover, both
71 small coccoliths and large coccoliths are useful in geochemical analyses (Ziveri et al., 2003; Rickaby
72 et al., 2010; Candelier et al., 2013; Bolton et al., 2012, 2016; Bolton and Stoll, 2013). Therefore,
73 both small and large coccoliths were studied in this research. (B). Pictures of the studied coccolith
74 are shown in Appendix B, and all classifications follow Nannotax3 except *Reticulofenestra* spp.
75 (Figure C2 in Appendix C).

76 **2.2 Experiment designs**

77 **2.2.1 Sample pretreatments**

78 The sinking velocity measurement depends on absolute abundance estimation (more details in 2.2.2).

79 However, on microscope slides, larger coccoliths and foraminifer fragments may cover smaller
80 coccoliths, reducing the accuracy of coccolith absolute numbers. Thus, before sinking experiments
81 were carried out, raw sediments were pretreated to purify the target coccoliths to reduce errors in
82 coccolith counting. The raw sediments were disaggregated in 0.2% ammonia and sieved through a
83 63 µm sieve and then treated by sinking method or filtering method (Bolton et al., 2012; Minoletti
84 et al., 2009) to concentrate the target species up to at least more than 50% of the total assemblage
85 (for Noëlaerhabdaceae coccoliths, a percentage more than 90% can be easily achieved). In one
86 sample with aggregation (ODP 807), we did a rapid settling (30 min, 2 cm) to eliminate aggregates.
87 Most of the species were measured individually in settling experiments, except for *Pseudoemiliana*
88 *lacunosa* and *Umbilicosphaera sibogae*, which were measured together.

89 **2.2.2 Measuring the sinking speeds of coccoliths**

90 We are not aware of any prior direct determination of the sinking velocity of individual coccoliths,
91 although the sinking velocities of live coccolithophores and other marine algal cells have been
92 successfully measured by the ‘FlowCAM’ method (Bach et al., 2012) or a similar photography
93 technique (e.g. Miklasz and Denny, 2010). Here we introduce a simple method to measure the
94 particle sinking speeds without special equipment.

- 95 1. After pretreatment, the coccolith suspensions were gently shaken and then moved into
96 comparison tubes which were vertically mounted on tube shelves. We set the timer going
97 and let the suspension settle for a specified period of time, marked as sinking time or
98 settling duration (T);
- 99 2. Thereafter, we removed the upper 15 ml supernatant into a 50 ml centrifuge tube with a 10
100 ml pipette. This operation was performed slowly and gently to avoid drawing lower
101 suspensions upward. The absolute counting of coccolith was achieved by using the ‘drop
102 technique’ to make quantitative microscope slides (Koch and Young, 2007; Bordiga et al.,
103 2015). 0.3 ml mixed suspension was extracted and pipettes onto a glass cover and dry the
104 slider on a hotplate;
- 105 3. The lower suspension was then homogenized and another slider was prepared as described
106 above;
- 107 4. The number of coccoliths in the upper and lower suspensions were carefully counted on

108 microscope at $\times 1250$ magnification and the number of coccoliths and fields of view (FOV)
109 were recorded for further calculations. More than 300 specimens were counted for most of
110 the measurements. For the *Helicosphaera carteri* measurements, more than 100 FOV were
111 checked and about 100 specimens were counted.

112 To calculate the sinking velocities of coccoliths, we define a parameter named the separation ratio
113 (R), which represents the percentage of removed coccoliths in one separation by pumping out the
114 upper suspension. This parameter is important and will be repeatedly mentioned in the following
115 part. R was measured using the following equation (more details about derivation can be found in
116 Appendix D):

$$117 \quad R = \frac{\frac{N_1}{n_1} \times V_1}{\frac{N_1}{n_1} \times V_1 + \frac{N_2}{n_2} \times V_2} \quad (2-1)$$

118 where N_1 and N_2 are numbers of coccoliths counted in upper and lower suspension slides,
119 respectively; n_1 and n_2 are the number of FOV counted. V_1 and V_2 are the volume of the settling
120 vessel defined by the settling distance, as shown in Figure 2.

121 The separation ratio, R, also has a relationship with sinking time, T (Appendix D):

$$122 \quad R = \frac{V_1 - \frac{V_1}{D} \times v \times T}{V_1 + V_2} \quad (2-2)$$

123 where V_1 , V_2 and D are shape parameters shown in Figure 2; and v is the average sinking velocity
124 of measured coccoliths. If we plot R against T, the slope of line has a relationship with v . Then liner
125 regressions between R and T were processed with MATLAB to calculate the v (details about error
126 analyses can be found in Appendix E).

127 There are still two issues to be explained. Firstly, to eliminate the shape differences among vessels,
128 all separation ratios have been transferred to calibrated separation ratios (R_{cal}), which means the
129 separation ratio measured in a standard vessel with $V_1=15$ ml, $V_2=10$ ml and $D=6$ cm (more details
130 about transformation from R to R_{cal} can be found in Appendix D). Secondly, we treated the average
131 sinking velocities as the sinking velocities of the coccoliths with the average length. This
132 approximation has been proved reasonable in Appendix D.

133 **2.2.3 Detecting the potential influence of vessels**

134 Seven commonly used vessels were selected to detect the potential influence of vessels (Figure 3).
135 Two of them are made of plastics (No.2 and No.3 in Figure 3) and all others are pyrex glass vessels.
136 About 500 mg of sediment from core KX21-2 were pretreated as described in 2.2.1 and suspended

137 in about 500 ml diluted ammonia. After that, settling experiments were performed as described in
138 2.2.2 using different vessels. In these experiments, only the dominant species, *G. oceanica*, was
139 measured.

140 **2.2.4 Other factors influencing the sinking velocity**

141 Temperature can change the density and viscosity of liquid. Generally speaking, the higher the
142 temperature is, the lower the density and viscosity will become and the faster pellets will sink. Take
143 water for instance, if the temperature increases from 15 to 30°C, the particle sinking velocity will
144 increase by ~43% (Table 1). All sinking velocities measured or discussed in the following sections
145 were velocities at 20°C to minimize the influence of temperature.

146 The calibration of sinking velocity in high concentration suspension has been calculated by
147 Richardson and Zaki (1954)

$$148 \quad v = v_0(1 - \alpha_s)^{2.7} \quad (2-3)$$

149 where the α_s is the solids volume fraction. Based on equation 2-3, the higher the suspension
150 concentration is, the slower the sinking velocity will be. That is so called ‘hindered settling’. When
151 the $\alpha_s=0.2\%$, the reduction of sinking velocity owing to hindered settling is negligible (v/v_0 equals
152 99.46%). Hence, in this study all suspensions have solid volume fractions lower than 0.2% to avoid
153 notable reductions of coccolith sinking velocities.

154 **3. Results and Discussions**

155 **3.1 Influence of vessels**

156 The sinking velocities of *G. oceanica* in the core KX21-2 in 0.2% ammonia at 20°C measured in
157 different vessels vary from 0.99 to 1.23 cm h⁻¹. The lowest value occurred in the 100 ml centrifuge
158 tube and the highest sinking velocity was measured in the 50 ml centrifuge tube experiments. The
159 correlations between sinking velocities and different vessel parameters are quite low: $r=0.13$ for the
160 vessel inner diameter, $r=0.0005$ for the sinking distance and $r=0.051$ for the upper volume and total
161 volume ratio ($V_1/(V_1+V_2)$). The dissipation of energy by friction between the moving fluid and the
162 walls can cause a reduction of sinking speed (wall effect). A significant wall effect will be detected
163 when a particle is settling in a vessel with a diameter that is smaller than 100 times of the particle
164 size (Barnea and Mizarchi, 1973). The length of coccoliths is on the micron scales, so the diameters

165 of vessel used in laboratory are more than four orders of magnitude larger than coccoliths. Moreover,
166 our results show that the difference between vessel materials, glass and plastics, can also be ignored
167 (Figure 4). Hence, we suggest that vessel type almost has no significant influence on sinking
168 velocity of coccoliths.

169 However, our experiments were premised on the basis that the concentration of suspension was
170 equal among different vessels. This means that large vessels can treat more sediment at one time but
171 if we choose a larger vessel, more suspensions should be pumped and it often costs more time in
172 sinking (often due to longer sinking distance). Assuming that the sediment is composed of 50%
173 calcite (with density of 2.7 g cm^{-3}) and 50% clay (about 1.7 g cm^{-3}), the largest amount of sediment
174 that can be used without significant reduction of the sinking velocity (5%) is about 400 mg in 100
175 ml suspension (this calculation is based on equation 2-3). However, because sediments accumulate
176 in the lower suspension, the particle concentration can be more than 4 times higher than in the initial
177 homogenous concentration. This phenomenon will be more significant for a vessel with a narrow
178 bottom, such as centrifuge tubes. To avoid this, we recommend using about 100 mg dry sediment
179 suspended in at least 100 ml suspension to avoid 'hindered settling'. If more sediment is necessary
180 for geochemistry analyses, then a larger vessel should be selected to separate enough sample at one
181 time.

182 **3.2 Sinking velocities at 20°C in 0.2% ammonia**

183 We measured the separation ratios of different coccoliths in comparison tubes at 20°C in 0.2%
184 ammonia (Figure 5). The sinking velocities of coccoliths were then calculated by linear fitting of
185 separation ratios and settling durations. The sinking velocities of studied coccoliths vary by two
186 orders of magnitude from 0.154 cm h^{-1} to 10.67 cm h^{-1} (Table 2). The highest sinking velocity was
187 found in the measurement of *Coccolithus pelagicus* and the lowest velocity was found for *F.*
188 *profunda*. The average sinking speed of coccoliths is about 10-50% of the terminal sinking velocities
189 of calcite spheres calculated by Stokes' Law (Figure 6c). These ratios are comparable to the oval
190 objects (e.g. seeds) data from Xie and Zhang (2001) and smaller than steel ellipsoids data from
191 McNown and Malaika (1950). The sinking velocities of coccoliths measured in our experiment are
192 about 2-3 orders of magnitude smaller than values from sediment traps of $143\text{-}243 \text{ m d}^{-1}$ ($595\text{-}1012$
193 cm h^{-1}) in the North Atlantic (Ziveri et al., 2000 and Stoll et al., 2007), suggesting that the coccoliths

194 sinking out of the euphotic layer are mainly in the form of sinking aggregates rather than individual
195 coccoliths.

196 **3.3 Estimating the sinking velocities**

197 Generally speaking, the sinking velocities of coccoliths increase with distal shield length (Figure
198 5a), as expected from the increase in volume to sectional area for a given geometry as length
199 increases. Our data implies that the sinking velocity has a power function relationship with distal
200 shield length.

201 We propose that the sinking velocity of coccoliths might have a quadratic relationship with distal
202 shield length as described by Stokes' Law (Figure 6a). If we use data for all species except *H. carteri*
203 (the reason can be found in the following discussion), the sinking velocities can be described by the
204 following equation:

$$205 \quad v = 0.0982 (\pm 0.001) * \phi^2 \quad (3-1)$$

206 Based on this quadratic regression, we derive a shape-velocity factor (k_v) that relates settling
207 velocity to coccolith length.

$$208 \quad v = k_v * \phi^2 \quad (3-2)$$

209 Furthermore, this factor is analogous to the shape-mass factor, ' k_s ' used to relate coccolith mass to
210 coccolith length (Young and Ziveri, 2000). The length and shape-velocity factor of coccoliths can
211 be used to predict most of the sinking velocity variations, however, variations may also arise due to
212 changes in coccolith mass and thickness, for a given length, and due to the hydrodynamics of
213 particular shapes. We noticed that the smaller coccolith *G. caribbeanica* has a greater sinking
214 velocity than the larger coccolith, *G. oceanica*. We suggest that this was caused by greater mass per
215 length (or greater average thickness) in the case of *G. caribbeanica* and this may be due to the closed
216 central area while *G. oceanica* has an open central area. Another example is *H. carteri*, which lower
217 sinking velocity of which can be explained by the unique structure of *H. carteri* coccolith. Firstly,
218 the broad edge of *H. carteri* can increase the drag force significantly. Moreover, most of the
219 measured coccoliths have a ellipticity (major axis length and minor axis length ratio) larger than 0.8,
220 while the ellipticity of *H. carteri* is around 0.6, which means the mass of *H. carteri* is smaller than
221 other species of coccoliths with similar lengths (Figure 6d and Figure C3). That is also the reason
222 *H. carteri* was excluded from the general regression in equation 3-1. In the case of partial dissolution,

223 the well-preserved *Cyclicargolithus floridanus* may have higher mass than dissolved (or
224 disarticulated) *C. floridanus*, and therefore a slightly higher shape-velocity factor.

225 **4. Suggestions for coccolith velocity estimations and separations**

226 To improve coccolith separation by settling methods, we measured sinking velocities of different
227 coccoliths by gravity. Sinking velocities in this study varied from 0.154 to 10.61 cm h⁻¹, about 10%
228 to 50% of those of calcite spheres with same diameter. The shape of different vessels had little
229 impact on the sinking velocity. But we should consider the volume of vessels to avoid ‘hindered
230 settling’. The sinking velocities are mainly controlled by the shape of coccolith, including the distal
231 shield length, the size of central area, and the ellipticity of coccoliths. Besides the shape of coccoliths,
232 temperature is also crucial to the coccolith separations because of the dependence of sinking
233 velocities on temperature. Length-velocity factors were proposed to estimate coccoliths sinking
234 velocities, so coccolith separation can be achieved by following steps:

- 235 1. Measure the length of coccoliths in your target assemblage under the microscope and
236 regress the length distribution by the assumption of normal distribution (details are in
237 Appendix C);
- 238 2. Estimate sinking velocities for each important species. For species which sinking speed
239 has been directly measured, we can use the length-velocity factor directly ($v=k_v \cdot \phi^2$).
240 For unmeasured species, we can choose the length-velocity factor of coccoliths with
241 similar morphology in this study or use the general length-velocity formula
242 ($v=0.098(\pm 0.001) \cdot \phi^2$);
- 243 3. Calculate the separation time for main species. For example, in KX21-2 there are three
244 main coccoliths, *F. profunda*, *G. oceanica* and *C. leptoporus* and we wish to separate *G.*
245 *oceanica* out from the bulk sediment. Calculate each coccoliths’ sinking velocity
246 distributions as described in Step 2 above. As shown in Figure 7, a sinking velocity
247 intermediate between *F. profunda* (with a length 2σ larger than average, marked as $+2\sigma$)
248 and *G. oceanica* (with a length 2σ smaller than average, marked as -2σ) optimal to
249 separate them, would be 0.6 cm h⁻¹. Similarly, we can chose speed thresholds 1.85 cm
250 h⁻¹ to separate *G. oceanica* from *C. leptoporus*. If we settle in a 50 ml centrifuge tube
251 with a sinking distance, *D*, equal to 5.84 cm, the sinking time for separating *F. profunda*

252 should be $T=5.84/0.6=9.73$ h. Similarly, we can calculate the time for separating *G.*
253 *oceanica* by $T=5.84/1.85=3.16$ h;

254 4. Homogenize the sediment suspension and let coccoliths settling as the period
255 calculated in Step 3. After that, pump out the upper part of suspension. In the upper
256 part, we have exclusively the smaller of the main coccoliths. However, column will
257 still contain some smaller ones. So this step (settling and pumping) should be repeated
258 until the lower part no longer has significant contribution from the smaller coccoliths.
259 This step has been well described in pervious studies and more details can be found in
260 Stoll and Ziveri (2002) and Bolton et al. (2012).

261 We find, if we use the general formula, a closed central area coccolith will sink faster than prediction
262 (for *G. caribbeanica* and small *C. leptoporus* will settle ~40% faster) and coccoliths with greater
263 ellipticity can settle much slower (for *H. carteri* will settle as 30% of the predicted sinking velocity
264 for coccolith with similar length). Moreover, the sinking method cannot separate every species of
265 coccoliths perfectly. As mentioned in Section 2.2.1, *P. lacunosa* and *U. sibogae* cannot easily be
266 separated from each other because they have similar sinking velocities. Nevertheless, this study
267 provides the first direct estimation of coccolith settling velocities, which should simplify
268 implementation of future methods to separate coccoliths by settling time.

269

270 *Acknowledgements.* This study was supported by grants from the Chinese National Science
271 Foundation (91428310, 91428309 and 41530964, to L.C.). We thank the Integrated Ocean Drilling
272 Program (IODP) for providing the samples. The IODP is sponsored by the U.S. National Science
273 Foundation and participating countries under management of the IODP Management International,
274 Inc (IODP-MI).

275 **Table 1.** The influence of temperature on sinking velocity. Density data is from Kell (1975) and
 276 viscosity data is from Joseph et al. (1978).

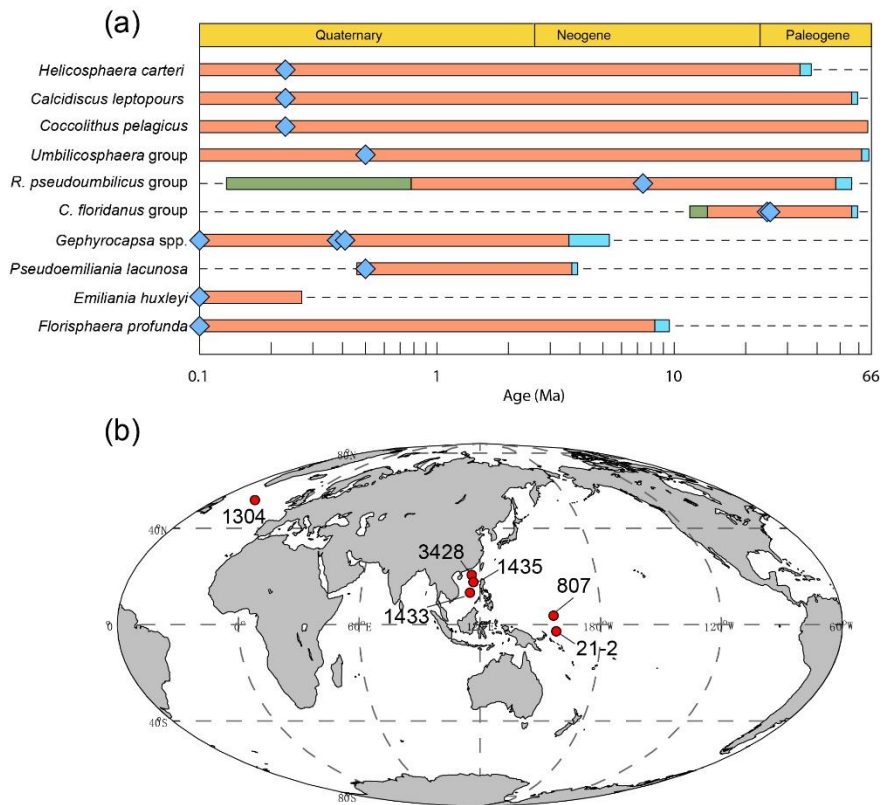
T (°C)	ρ (g cm ⁻³)	η (mPa s)	$v_T : v_{T=20}$
15	0.9991	1.1447	0.8804
20	0.9982	1.0087	1
25	0.9970	0.8949	1.1279
30	0.9956	0.8000	1.2627

277 **Table 2.** The sinking velocity and shape-velocity factor of different coccolith species: ϕ means the
 278 distal shield length of coccolith and St ϕ is the standard deviation of distal shield length; sv represents
 279 the sinking velocity; v (95%-) and v (95%+) represent the lower and higher limit of 95% confidence
 280 level, respectively. 'k_v' represents the length-sinking velocity factor. The short name of coccolith can be
 281 found in the caption of Figure 4. The details of coccoliths length distribution are in Appendix C.

Species	abb.	ϕ (μm)	St ϕ (μm)	sinking velocity (cm h ⁻¹)	v (95% -)	v (95% +)	k _v
<i>F. profunda</i>	Fp-WP	1.508	0.557	0.158	0.010	0.011	0.070
<i>F. profunda</i>	Fp-SCS	1.786	0.641	0.154	0.051	0.052	0.048
small <i>Reticulofenestra</i>	Ret (<4um)	2.454	0.509	0.848	0.354	0.416	0.141
<i>E. huxleyi</i>	Emi	2.512	0.469	0.853	0.054	0.064	0.135
<i>Gephyocapsa</i> spp.	G spp	2.755	0.502	0.752	0.125	0.147	0.099
<i>G. caribbeanica</i>	Gcar	3.312	0.352	1.873	0.174	0.192	0.171
<i>U. sibogae</i>	Umb	4.060	0.500	1.268	0.416	0.441	0.077
<i>G. oceanica</i>	Geo	4.187	0.517	1.170	0.155	0.178	0.067
<i>P. lacunosa</i>	Pla	4.350	0.617	1.171	0.337	0.338	0.062
Small <i>C. leptoporus</i>	Cal small	4.605	0.629	3.351	0.172	0.199	0.158
large <i>Reticulofenestra</i>	Ret(>4um)	4.988	0.605	2.379	0.534	0.641	0.096
<i>C. floridanus</i>	Cyf	5.805	0.963	4.174	0.320	0.336	0.124
(dissolved) <i>C. floridanus</i>	Cyf -d	6.134	0.727	4.508	0.352	0.417	0.120
Large <i>C. leptoporus</i>	Cal large	6.370	0.931	3.737	1.053	1.336	0.092
<i>H. carteri</i>	Hel	8.936	0.994	2.541	1.740	2.440	0.032
<i>C. pelagicus</i>	Cpl	10.640	1.175	10.610	0.950	1.235	0.094

282

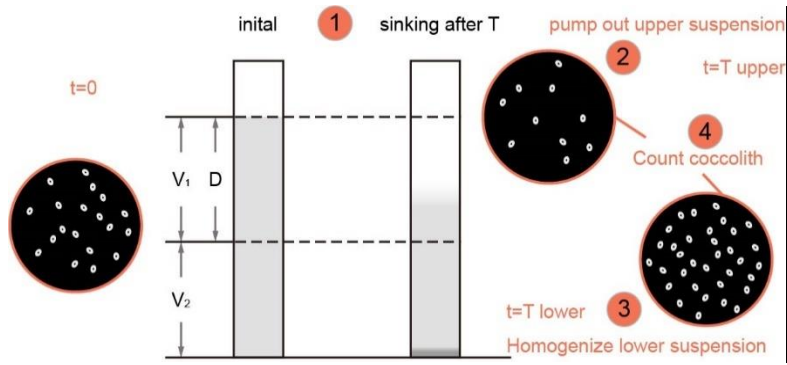
283 **Figure 1.** Temporal and spatial distribution of samples. (a) The evolution of studied coccoliths: first
 284 occurrence and last occurrence data are from Nannotax3
 285 (<http://www.mikrotax.org/Nannotax3/index.html>). The blue bars represent ranges of first occurrence
 286 and the green bars represent ranges of last occurrence. The blue diamonds represent samples used in
 287 this study. (b) Spatial distribution of samples. 1304 means IODP U1304, 3428 means MD12-3428cq,
 288 1433 and 1435 means IODP U1433 and U1435, respectively. 807 means ODP 807 and 21-2 means
 289 KX21-2.



290

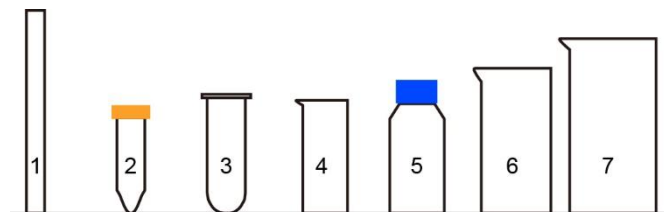
291

292 **Figure 2.** Schematic of settling experiments. V_1 and V_2 are the volumes of the upper and lower
293 cylinders, D is the settled distance. The numbers in circles are same as the number of Steps described in
294 Section 2.2.1.



295

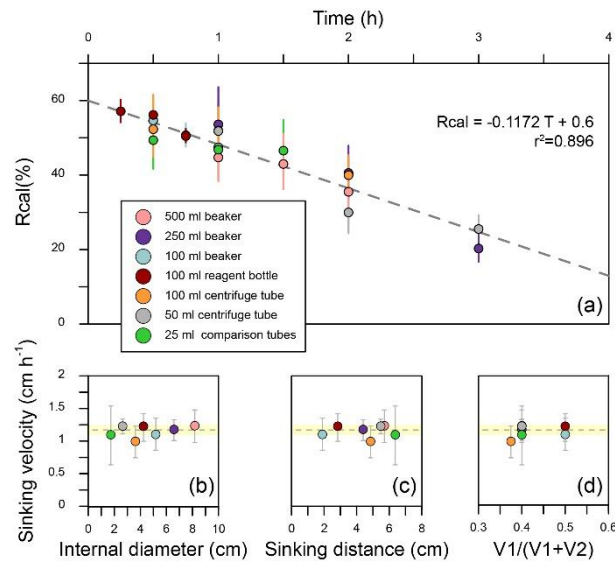
296 **Figure 3.** The shape parameters of vessels. V_1 and V_2 means the volume of upper suspension and lower
 297 suspension, respectively. D means sinking distance. Φ means average inner diameter which is
 298 calculated by $2*(V_1/\pi D)^2$.



No.	Name	V1	V2	D (cm)	Φ (cm)
1	25 ml comparison tube	15	10	6.376	1.73
2	50 ml centrifuge tube	30	20	5.480	2.64
3	100 ml centrifuge tube	50	30	4.854	3.62
4	100 ml beaker	40	40	2.834	4.24
5	100 ml reagent bottle	40	40	1.900	5.18
6	250 ml beaker	150	100	4.400	6.59
7	500 ml beaker	300	200	5.700	8.19

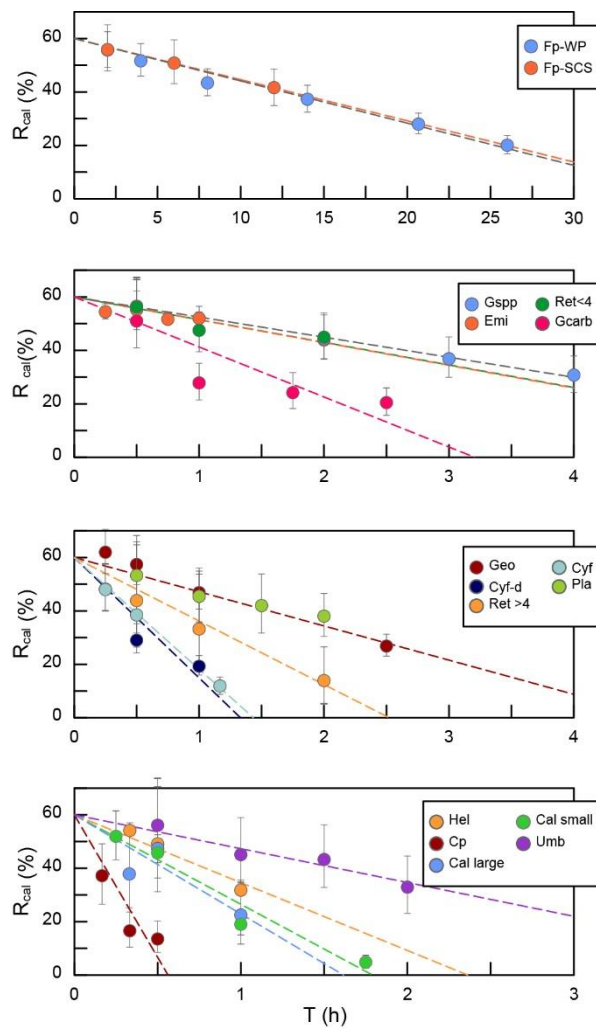
299
 300

301 **Figure 4.** Sinking velocities of *G. oceanica* in the core KX-21-2 measured in different vessels. (a) The
 302 calibrated separation ratios measured in different vessels. Error bars show 95% confidence level of
 303 calibrated separation ratio. (b-d) The relationship between sinking velocity and different vessel shape
 304 parameters. Error bars represent 95% confidence level of sinking velocity in each vessel and the shade
 305 area represents 95% confidence level of sinking velocity considering all data points.



306

307 **Figure 5.** The calculated separation ratio (R_{cal}) vs sinking duration. Fp-WP means *F. profunda* in the
 308 West Pacific. Fp-SCS means *F. profunda* in the South China Sea. Emi means *E. huxleyi*. Gspg means
 309 small *Geophyocapsa*. Geo means *G. oceanica*. Gcarb means *G. caribbeanica*. Ret<4 means small
 310 *Reticulofenestra*. Ret>4 means large *Reticulofenestra*. Cyf means *Cyclicargolithus floridanus*. Cy-d
 311 means dissolved *C. floridanus*. Umb means *U. sibogae*. Pla means *Pseudoemiliana lacunosa*. Hel
 312 means *H. carteri*. Cal large means larger *Calcidiscus leptoporus*. Cal small means small *C. leptoporus*.
 313 Cpl means *C. pelagicus*.

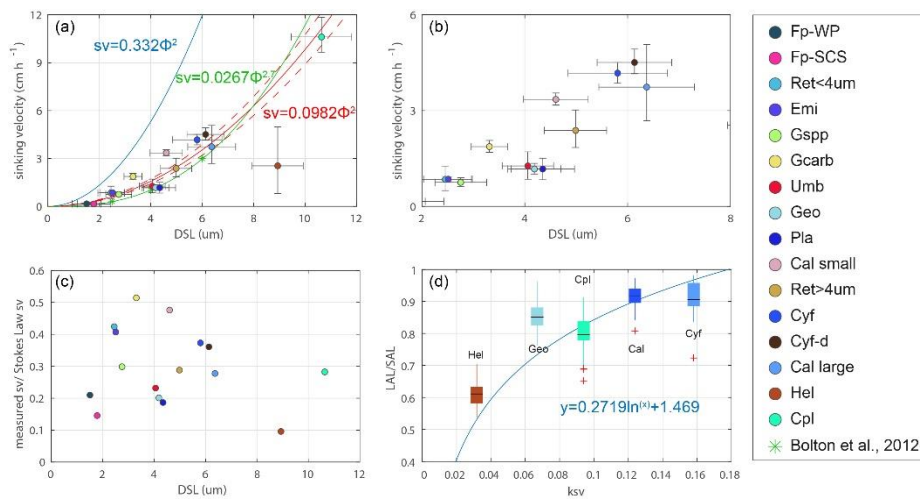


314

315

316

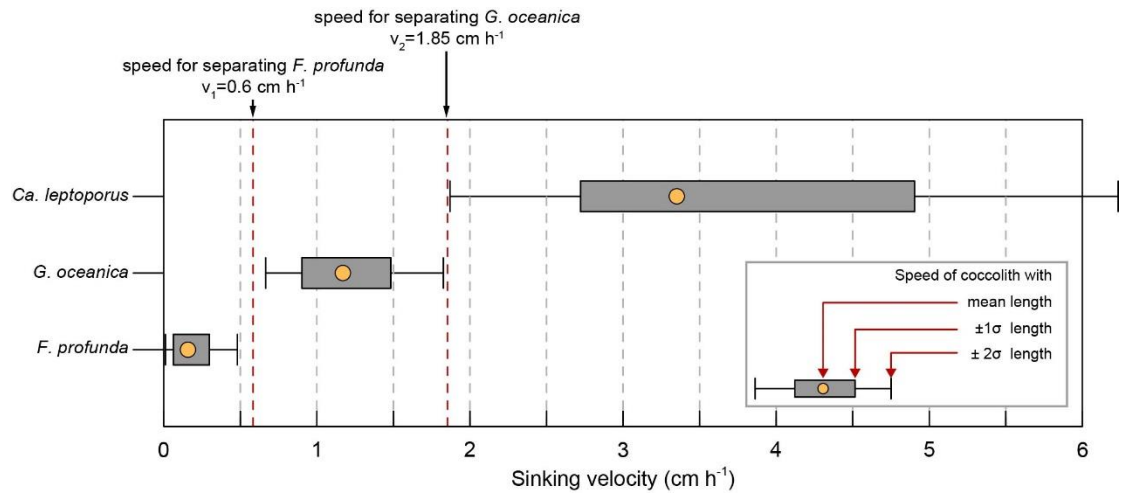
317 **Figure 6.** Coccolith sinking velocities and coccolith shape factors. (a-b) Sinking velocities and mean
318 distal shield length. The horizontal error bars represent one standard deviation of coccolith length and
319 the vertical ones represent 95% confidence level of measured sinking velocities. The blue, green and
320 red lines represent sinking velocity of calcite sphere objects, coccolith sinking velocities estimated by
321 Bolton et al. (2012) and this study, respectively. (c) The ratio of measured speed and speed calculated
322 by Stokes' Law. (d) Coccolith short axis length (SAL) and long axis length (LAL) ratio against shape-
323 velocity factor k_v . Box shows median value and upper/lower quartiles, whiskers show maximum and
324 minimum values, outliers larger than 1.5 of the interquartile range are shown as red crosses. The SAL
325 against LAL plot was shown in Figure C3. The short names of coccoliths can be found in Table 2.



326

327

328 **Figure 7.** The selection of separation velocities: the sinking velocities of three main coccolith species
 329 in sample from core KX21-2 were calculated by the length distribution and velocity factors in Table 2.
 330 The yellow dots represent sinking velocities of coccoliths with mean length. The edge of boxes show
 331 the sinking velocities of coccolith within one standard deviation of length ($\pm 1\sigma$) and the whiskers
 332 mark the sinking velocities of coccolith within two standard deviation of length ($\pm 2\sigma$).



333

334 **References**

- 335 Bach, L.T., Riebesell, U., Sett, S., Febiri, S., Rzepka, P., Schulz, K.G., 2012. An approach for
336 particle sinking velocity measurements in the 3-400 μm size range and considerations on
337 the effect of temperature on sinking rates. *Mar Biol* 159, 1853-1864, doi:10.1007/s00227-
338 012-1945-2.
- 339 Barnea, E., Mizrahi, J., 1973. A generalized approach to the fluid dynamics of particulate
340 systems: Part 1. General correlation for fluidization and sedimentation in solid
341 multiparticle systems. *The Chemical Engineering Journal* 5, 171-189, doi:10.1016/0300-
342 9467(73)80008-5.
- 343 Baumann, K.-H., 2004. Importance of size measurements for coccolith carbonate flux estimates.
344 *Micropaleontology*, 35-43.
- 345 Beaufort, L., Lancelot, Y., Camberlin, P., Cayre, O., Vincent, E., Bassinot, F., Labeyrie, L.,
346 1997. Insolation cycles as a major control of equatorial Indian Ocean primary production.
347 *Science* 278, 1451-1454, doi:10.1126/science.278.5342.1451.
- 348 Beltran, C., de Rafélis, M., Minoletti, F., Renard, M., Sicre, M.A., Ezat, U., 2007. Coccolith
349 $\delta^{18}\text{O}$ and alkenone records in middle Pliocene orbitally controlled deposits: High-
350 frequency temperature and salinity variations of sea surface water. *Geochemistry,*
351 *Geophysics, Geosystems* 8, Q05003, doi:10.1029/2006GC001483.
- 352 Bolton, C.T., Hernandez-Sanchez, M.T., Fuertes, M.A., Gonzalez-Lemos, S., Abrevaya, L.,
353 Mendez-Vicente, A., Flores, J.A., Probert, I., Giosan, L., Johnson, J., Stoll, H.M., 2016.
354 Decrease in coccolithophore calcification and CO_2 since the middle Miocene. *Nat*
355 *Commun* 7, 10284, doi:10.1038/ncomms10284.
- 356 Bolton, C.T., Stoll, H.M., 2013. Late Miocene threshold response of marine algae to carbon
357 dioxide limitation. *Nature* 500, 558-562, doi:10.1038/nature12448.
- 358 Bolton, C.T., Stoll, H.M., Mendez-Vicente, A., 2012. Vital effects in coccolith calcite:
359 Cenozoic climate- pCO_2 drove the diversity of carbon acquisition strategies in
360 coccolithophores, *Paleoceanography* 27, doi:10.1029/2012pa002339.
- 361 Bordiga, M., Bartol, M., Henderiks, J., 2015. Absolute nannofossil abundance estimates:
362 Quantifying the pros and cons of different techniques. *Revue de micropaléontologie* 58,

363 155-165 doi:10.1016/j.revmic.2015.05.002.

364 Candelier, Y., Minoletti, F., Probert, I., Hermoso, M., 2013. Temperature dependence of
365 oxygen isotope fractionation in coccolith calcite: A culture and core top calibration of the
366 genus *Calcidiscus*. *Geochimica et Cosmochimica Acta* 100, 264-281,
367 doi:10.1016/j.gca.2012.09.040.

368 Hermoso, M., Candelier, Y., Browning, T.J., Minoletti, F., 2015. Environmental control of the
369 isotopic composition of subfossil coccolith calcite: Are laboratory culture data transferable
370 to the natural environment? *GeoResJ* 7, 35-42, doi:10.1016/j.grj.2015.05.002.

371 Hermoso, M., Chan, I.Z.X., McClelland, H.L.O., Heures, A.M.C., Rickaby, R.E.M., 2016.
372 Vanishing coccolith vital effects with alleviated carbon limitation. *Biogeosciences* 13,
373 301-312, doi:10.5194/bg-13-301-2016.

374 Jin, X., Liu, C., Poulton, A.J., Dai, M., Guo, X., 2016. Coccolithophore responses to
375 environmental variability in the South China Sea: species composition and calcite content.
376 *Biogeosciences* 13, 4843-4861, doi: 10.5194/bg-13-4843-2016.

377 Kell, G.S., 1975. Density, thermal expansivity, and compressibility of liquid water from 0. deg.
378 to 150. deg.. correlations and tables for atmospheric pressure and saturation reviewed and
379 expressed on 1968 temperature scale. *Journal of Chemical and Engineering Data* 20, 97-
380 105.

381 Kestin, J., Sokolov, M., Wakeham, W.A., 1978. Viscosity of liquid water in the range -8°C to
382 150°C . *Journal of Physical and Chemical Reference Data* 7, 941-948.

383 Koch, C., Young, J., 2007. A simple weighing and dilution technique for determining absolute
384 abundances of coccoliths from sediment samples. *J. Nanoplankton Res.*

385 McClelland, H.L., Bruggeman, J., Hermoso, M., Rickaby, R.E., 2017. The origin of carbon
386 isotope vital effects in coccolith calcite. *Nat Commun* 8, 14511,
387 doi:10.1038/ncomms14511.

388 McClelland, H.L., Barbarin, N., Beaufort, L., Hermoso, M., Ferretti, P., Greaves, M., Rickaby,
389 R.E.M., 2016. Calcification response of a key phytoplankton family to millennial-scale
390 environmental change. *Scientific Reports* 6, 34263, doi: 10.1038/srep34263.

391 McNown, John S., and Jamil Malaika. "Effects of particle shape on settling velocity at low

392 Reynolds numbers." *Eos, Transactions American Geophysical Union* 31.1 (1950): 74-82.

393 Miklasz, K.A., Denny, M.W., 2010. Diatom sinkings speeds: Improved predictions and insight
394 from a modified Stokes' law. *Limnology and Oceanography* 55, 2513-2525,
395 doi:10.4319/lo.2010.55.6.2513.

396 Minoletti, F., Hermoso, M., Gressier, V., 2009. Separation of sedimentary micron-sized
397 particles for palaeoceanography and calcareous nannoplankton biogeochemistry. *Nat.*
398 *Protocols* 4, 14-24, doi:10.1038/nprot.2008.200.

399 Paull, C.K., Thierstein, H.R., 1987. Stable isotopic fractionation among particles in Quaternary
400 coccolith-sized deep-sea sediments. *Paleoceanography* 2, 423-429,
401 doi:10.1029/PA002i004p00423.

402 Edwards, A.R., 1963. A preparation technique for calcareous nannoplankton.
403 *Micropaleontology* 9, 103-104.

404 Richardson, J., Zaki, W., 1954. The sedimentation of a suspension of uniform spheres under
405 conditions of viscous flow. *Chemical Engineering Science* 3, 65-73.

406 Rickaby, R.E.M., Henderiks, J., Young, J.N., 2010. Perturbing phytoplankton: response and
407 isotopic fractionation with changing carbonate chemistry in two coccolithophore species.
408 *Clim. Past* 6, 771-785, doi:10.5194/cp-6-771-2010.

409 Rousselle, G., Beltran, C., Sicre, M.-A., Raffi, I., De Raféllis, M., 2013. Changes in sea-surface
410 conditions in the Equatorial Pacific during the middle Miocene–Pliocene as inferred from
411 coccolith geochemistry. *Earth and Planetary Science Letters* 361, 412-421,
412 doi:10.1016/j.epsl.2012.11.003.

413 Sprengel, C., Baumann, K.-H., Henderiks, J., Henrich, R., Neuer, S., 2002. Modern
414 coccolithophore and carbonate sedimentation along a productivity gradient in the Canary
415 Islands region: seasonal export production and surface accumulation rates. *Deep Sea*
416 *Research Part II: Topical Studies in Oceanography* 49, 3577-3598 doi: 10.1016/S0967-
417 0645(02)00099-1.

418 Stoll, H.M., 2005. Limited range of interspecific vital effects in coccolith stable isotopic records
419 during the Paleocene-Eocene thermal maximum. *Paleoceanography* 20,
420 doi:10.1029/2004pa001046.

421 Stoll, H.M., Rosenthal, Y., Falkowski, P., 2002. Climate proxies from Sr/Ca of coccolith calcite:
422 calibrations from continuous culture of *Emiliana huxleyi*. *Geochimica et Cosmochimica*
423 *Acta* 66, 927-936, doi:10.1016/S0016-7037(01)00836-5.

424 Stoll, H.M., Ziveri, P., 2002. Separation of monospecific and restricted coccolith assemblages
425 from sediments using differential settling velocity. *Marine Micropaleontology* 46, 209-
426 221, doi: 10.1016/S0377-8398(02)00040-3.

427 Xie, H-Y., and D-W. Zhang. "Stokes shape factor and its application in the measurement of
428 spherity of non-spherical particles." *Powder Technology* 114.1 (2001): 102-105 doi:
429 10.1016/S0032-5910(00)00269-2.

430 Young, J.R., Ziveri, P., 2000. Calculation of coccolith volume and it use in calibration of
431 carbonate flux estimates. *Deep sea research Part II: Topical studies in oceanography* 47,
432 1679-1700, doi:10.1016/S0967-0645(00)00003-5.

433 Zhang, H., Liu, C., Jin, X., Shi, J., Zhao, S., Jian, Z., 2016. Dynamics of primary productivity
434 in the northern South China Sea over the past 24,000 years. *Geochemistry, Geophysics,*
435 *Geosystems* 17, 4878-4891, doi:10.1002/2016GC006602 .

436 Ziveri, P., Stoll, H., Probert, I., Klaas, C., Geisen, M., Ganssen, G., Young, J., 2003. Stable
437 isotope 'vital effects' in coccolith calcite. *Earth and Planetary Science Letters* 210, 137-
438 149, doi:10.1016/S0012-821X(03)00101-8.

439 **Appendix A. Sample selections**

440 **Table A1.** Sample selections

Measured coccolith	abb.	Region	Core	Section	Epoch	Age model ref.
<i>F. profunda</i>	Fp-SCS	SCS	MD12-3428	0-1 cm	Holocene	Zhang et al., 2016
<i>F. profunda</i>	Fp-WP	W.P.	KX21-2	2-4 cm	Holocene	Liang et al., 2016
<i>E. huxleyi</i>	Emi	SCS	MD12-3428	0-1 cm	Holocene	Zhang et al., 2016
<i>Gephyocapsa</i> spp.	Gspp	W.P.	ODP 807A	1H 5W 102-104	Pleistocene	Jin et al., 2010
<i>G. oceanica</i>	Geo	W.P.	KX21-2	2-4 cm	Holocene	Liang et al., 2016
<i>G. caribbeanica</i>	Gcarb	N.A.	IODP 1304B	7H 5W 69-70	Pleistocene	Channell et al., 2010
small <i>Reticulofenestra</i>	Ret<4	SCS	IODP 1433B	28R 2W 30-34	Miocene	Li et al., 2013
large <i>Reticulofenestra</i>	Ret>4	SCS	IODP 1433B	28R 2W 30-34	Miocene	Li et al., 2013
<i>Cyclicargolithus floridanus</i>	Cyf	SCS	IODP 1435A	6R 3W 25-29	Oligocene	Li et al., 2013
<i>Cyclicargolithus floridanus</i>	Cyf-d	SCS	IODP 1435A	8R 1W 27-31	Oligocene	Li et al., 2013
<i>Umbilicosphaera sibogae</i>	Umb	W.P.	ODP 807A	3H 5W 92-94	Pleistocene	Jin et al., 2010
<i>Pseudoemiliana lacunosa</i>	Pla	W.P.	ODP 807A	3H 5W 92-94	Pleistocene	Jin et al., 2010
<i>Helicosphaera carteri</i>	Hel	W.P.	ODP 807A	3H 5W 92-94	Pleistocene	Jin et al., 2010
large <i>Calcidiscus leptoporus</i>	Cal large	W.P.	ODP 807A	3H 5W 92-94	Pleistocene	Jin et al., 2010
small <i>Calcidiscus leptoporus</i>	Cal small	N.A.	IODP 1304B	7H 5W 69-70	Pleistocene	Channell et al., 2010
<i>Coccolithus pelagicus</i>	Cpl	N.A.	IODP 1304B	7H 5W 69-70	Pleistocene	Channell et al., 2010

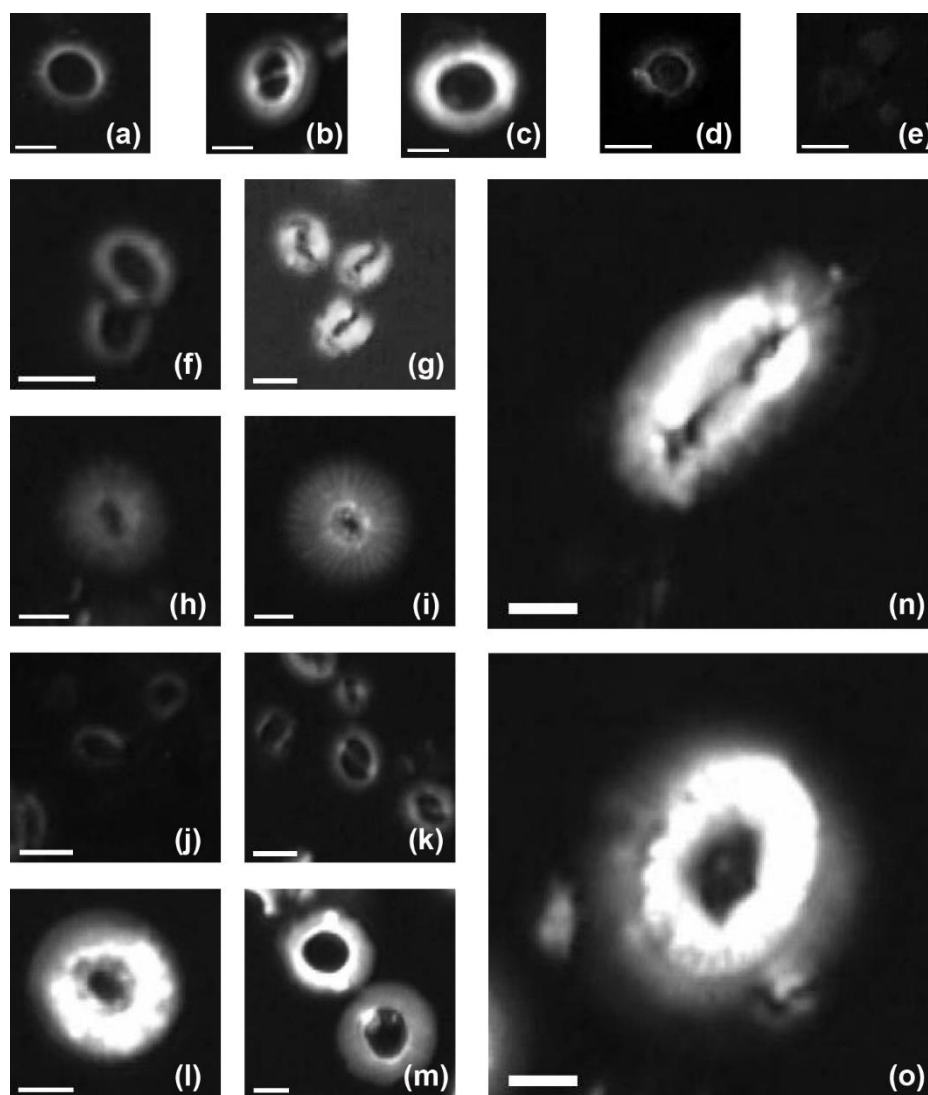
441

442 **References:**

- 443 Channell, J., Sato, T., Kanamatsu, T., Stein, R., Alvarez Zarikian, C., 2010. Expedition
444 303/306 synthesis: North Atlantic climate. Channell, JET, Kanamatsu, T., Sato, T., Stein,
445 R., Alvarez Zarikian, CA, Malone, MJ, and the Expedition 303, 306.
- 446 Jin, H., Jian, Z., Cheng, X., Guo, J., 2011. Early Pleistocene formation of the asymmetric
447 east-west pattern of upper water structure in the equatorial Pacific Ocean. Chinese
448 Science Bulletin 56, 2251-2257.

- 449 Li, C.-F., Lin, J., Kulhanek, D.K., 2013. South China Sea tectonics: Opening of the South
450 China Sea and its implications for southeastAsian tectonics, climates, and deep mantle
451 processes since the late Mesozoic. IODP Sci. Prosp 349.
- 452 Liang, D., Liu, C., 2016. Variations and controlling factors of the coccolith weight in the
453 Western Pacific Warm Pool over the last 200 ka. Journal of Ocean University of China
454 15, 456-464.
- 455 Zhang, H., Liu, C., Jin, X., Shi, J., Zhao, S., Jian, Z., 2016. Dynamics of primary productivity
456 in the northern South China Sea over the past 24,000 years. Geochemistry, Geophysics,
457 Geosystems 17, 4878-4891.

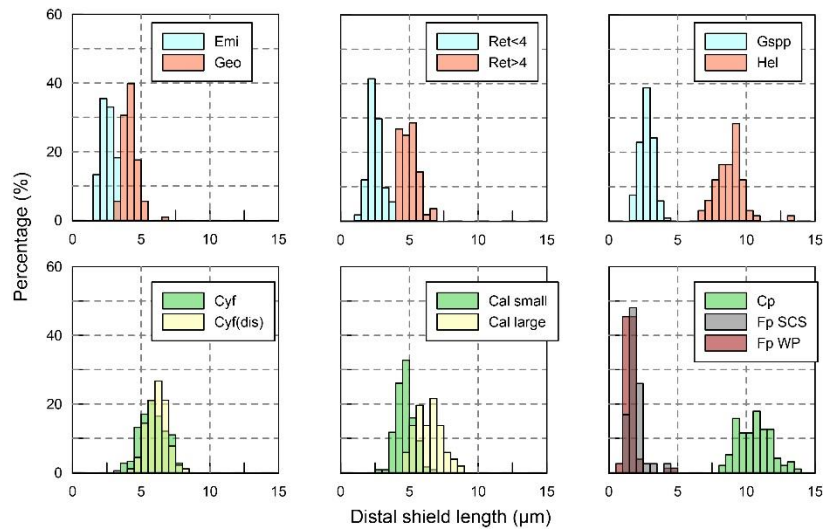
458 **Appendix B. Coccolith images under circular polarized light**



459
 460 **Plate B1.** Imaged of measured coccolith in this study: (a) *Pseudoemiliania lacinosa* in the core ODP
 461 807; (b) *Gephyrocapsa oceanica* in the core KX21-2; (c) *Reticulofenestra* spp. (large) in the core
 462 IODP U1433B; (d) *Umbilicosphaera sibogae* in the core ODP 807; (e) *Florisphaera profunda* in
 463 the core KX21-2; (f) *Reticulofenestra* spp. (small) in the core IODP U1433B; (g) *Gephyrocapsa*
 464 *caribbeanica* in the core IODP U1304B; (h) small *Calcidiscus leptoporus* in the core IODP U1304B;
 465 (i) large *Calcidiscus leptoporus* in the core ODP 807A; (j) *Emiliana huxleyi* in the surface sediment
 466 in the South China Sea; (k) *Gephyrocapsa* spp. in the core ODP 807; (l) *Cyclicargolithus floridanus*
 467 in the core IODP U1435A and (m) dissolved *Cyclicargolithus floridanus* in the same core; (n)
 468 *Helicosphaera carteri* in the core ODP 807A; (o) *Coccolithus pelagicus* in the core IODP U1304B.
 469 White bars represent a length of 2 μ m.

470 **Appendix C. The length distribution of coccoliths**

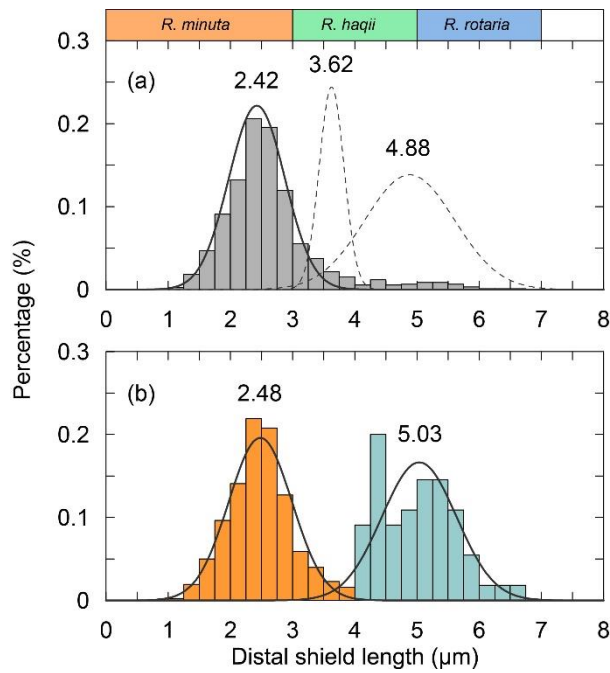
471 To measure the distal shield length of coccoliths, pictures were taken at a magnification of 1250x
472 under circular polarized light. The coccolith lengths were measured by using the image analysis
473 software, ImageJ. More than 5 pictures were taken and more than 50 (usually more than 100)
474 coccolith specimens were measured. The length distributions of coccoliths measured in our
475 experiments were shown in the Figure C1.



476

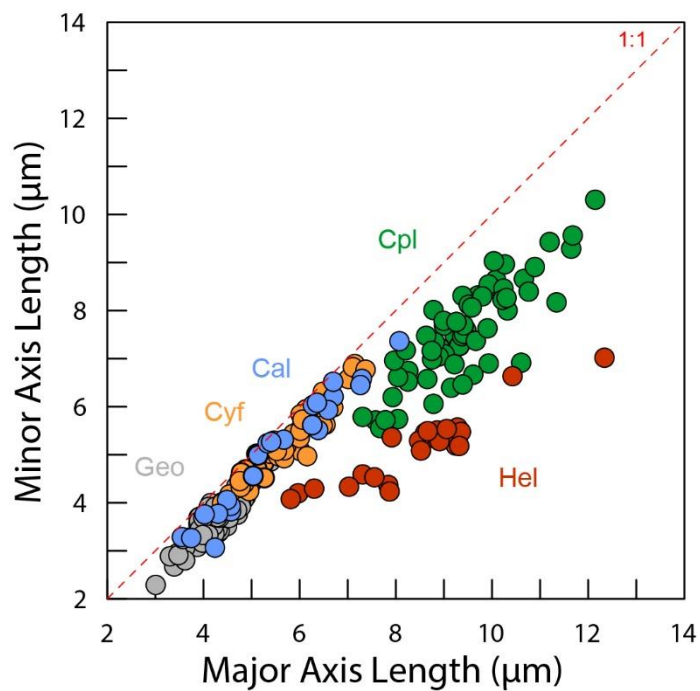
477 **Figure C1.** Size distribution of coccolith measured in the present study. The shorten names of coccolith
478 follow Table A1.

479 The classification of coccoliths by length was supported by mixture analysis in PAST (Hammer et
480 al., 2001), such as *Reticulofenestra* spp. and *Gephyrocapsa* spp. *Reticulofenestra* spp. in the
481 Miocene were classified into two groups, Ret. (<4 µm) and Ret. (>4 µm). The traditional
482 classification of *Reticulofenestra* spp. is <3 µm, 3-5 µm and 5-7 µm didn't pass the normal
483 distribution test. Hence, in this study the *Reticulofenestra* spp. are divided at 4 µm (Figure C2).
484 *Gephyrocapsa* spp. were classified by the shape of coccoliths into small *Gephyrocapsa* (central area
485 opening and length <3.5 µm), *G. oceanica* (central area opening and length >3.5µm) and *G.*
486 *caribbeanica* (closed central area) by the length and central area.



487

488 **Figure C2.** The classical classification of *Reticulofenestra* spp. (a) and the classification used in our
 489 study (b). The curves represent the normal distribution fits of different coccolith groups and the dish
 490 curve marks that the goodness of fit is below 0.2.



491

492 **Figure C3.** The short axis and long axis length distribution of coccoliths in Figure 6d.

493 **Reference.**

494 Hammer, Ø., Harper, D., Ryan, P., 2001. Paleontological Statistics Software: Package for
495 Education and Data Analysis. *Palaeontologia Electronica*.

496 **Appendix D. Coccolith movement in gravity settling**

497 In this part, the derivation of equation will be explained in detail including proofs of several
498 assumptions mentioned in the methods part.

499 When the well mixed sediment begins to sink, the decrease of coccoliths number in the upper
500 suspension (N_u) can be described as following equation:

$$501 \quad \frac{dN_u}{dT} = -\frac{N_{u(t=0)}}{D} \times v \quad (\text{D-1})$$

502 where the D is the length of upper suspension and $N_{u(t=0)}/D$ is the initial number of coccolith in
503 cross-section with a unit thickness, v is the mean sinking velocity of coccolith. In practice, the
504 velocities of coccoliths are different, so we assume the measured velocity is the mean sinking
505 velocity of bulk coccolith. This assumption will be proved valid in the following. The particle can
506 reaches 99.9% of the maximum sinking velocity within only 10^{-7} s, so we assume the particle sinks
507 as maximum velocity from the beginning of its settling.

508 Do integration for the equation D-1, we can get the variation of coccolith number in the upper
509 column over time:

$$510 \quad N_u = N_{u(t=0)} - \frac{N_{u(t=0)}}{D} \times v \times T \quad (\text{D-2})$$

511 where T is settling time. After a period of time (T), we pump out the upper suspension. Here we
512 define the number of coccoliths in the upper supernatant dividing the total coccoliths number in the
513 tube (N_t) as separation ratio (R), which represents the percentage of total coccoliths removed in one
514 separation. R can be expressed by

$$515 \quad R = \frac{N_u}{N_t} \quad (\text{D-3})$$

516 Assuming all coccoliths are uniformly distributed in the suspension at the beginning of settling,

517 $N_{u(t=0)}$ has relationship with N_t as follow:

$$518 \quad \frac{N_{u(t=0)}}{N_t} = \frac{V_1}{V_1+V_2} \quad (\text{D-4})$$

519 where V_1 is the volume of upper suspensions and V_2 is the volume of lower suspensions.

520 Combining the equation D-1, D-2, D-3 and D-4, we obtain the relationship between separation ratio,
521 R , and sinking velocity, v , as follow:

$$522 \quad R = \frac{N_u}{N_t} = \frac{N_{u(t=0)} - \frac{N_{u(t=0)}}{D} \times v \times T}{N_t} = \frac{V_1 - \frac{V_1}{D} \times v \times T}{V_1+V_2} \quad (\text{D-5})$$

523 If we plot the R and T on a figure, the slope of the line is a function of V_1 , V_2 , D and v . Since the

524 V_1, V_2, D are known parameters, we say the slope of R-T is a function of v , which is exactly what
525 we want.

526 Comparison tubes used in our experiments have the same V_1 and V_2 but different D . Other vessels
527 used in other experiments have different V_1, V_2 and D . So we should adjust the raw separation ratio
528 to calibrated separation ratio (R_{cal}), which represents the separation ratio made in a standard vessel
529 with $V_{1std}=15$ ml, $V_{2std}=10$ ml and $D_{std}=6$ cm. This step can be described by equation D-6:

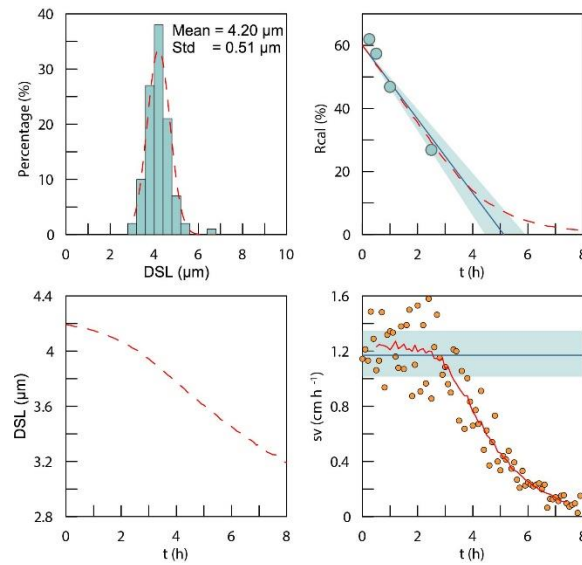
$$530 \quad R_{cal} = \frac{[R \times (V_1 + V_2) - V_1] \times D \times V_{1std}}{(D_{std} \times V_1 + V_{1std}) \times (V_{1std} + V_{2std})} \quad (D-6)$$

531 After calibrated, the slope of R_{cal} -T (k) has relationship with v as following equation:

$$532 \quad v = -\frac{D_{std} \times (V_{1std} + V_{2std})}{V_{1std}} \times k = -10 \times k \quad (D-7)$$

533 where k is the slope of R_{cal} against T from regression and other parameters are as described above.
534 Hence, the sinking velocity of different coccoliths can be achieved by measuring the variations of
535 R_{cal} over time.

536 The coccoliths' lengths in the sediment have some variations. So what we measured is actually the
537 bulk settling velocity of whole coccolith population. We also offer a test for the assumption that the
538 average sinking velocity of all coccoliths can be treated as the sinking velocity of coccoliths with
539 the average length. Here we used the data of *G. oceanica*. A normal distribution was fitted to the
540 measured length distribution (Figure D1-a). We generated 100000 coccolith following the normal
541 distribution and let these coccolith evenly distributing in the comparison tube at the initial and then
542 set them sinking without collisions with each other. The sinking velocities of different size
543 coccoliths were calculated by the velocity-shape parameter ' k_v ' as described in discussion part. We
544 modeled the coccoliths sinking process and computed the separation ratio (red dash line in Figure
545 D1-b), coccolith length (red dash line in Figure D1-c) and instant sinking velocities (orange dots in
546 Figure D1-d) at different time sections.



547

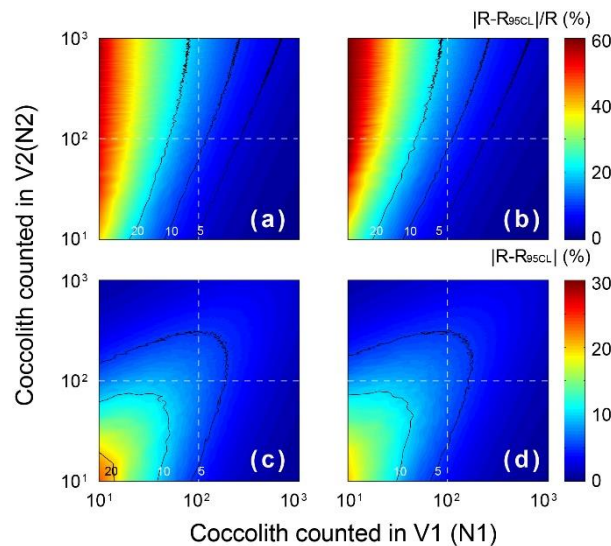
548

549 **Figure D1.** The simulations of coccoliths settling with different lengths: (a) the length distribution of
 550 coccoliths. The green bars represent measured data and red dash line represents the best fit for normal
 551 distribution. (b) The calibrated separation ratio: the green dots are measured data in our settling
 552 experiments, the blue line and shade area represent the calculated sinking velocity based on R_{cal}
 553 measurement and the red dash line represents results obtained from simulations. (c) The average length
 554 of removed coccolith in simulations; (d) the modeling sinking velocities of coccoliths: the orange dots
 555 are instant sinking velocity calculated from derivation of R_{cal} , the red dash line is weighted average for
 556 the instant sinking velocity. Blue line represents the average sinking velocity we measured and the
 557 green shade area represents 95% confidence level of the measured velocity.

558 For *G. oceanica* experiments, the instant sinking velocity would not change significantly until
 559 settling for more 3 hours. That means for all R_{cal} larger than 15% are safe for liner regressions. The
 560 minimum safe number of R_{cal} will descend with the drop of dispersion degree of coccolith length
 561 distribution. Hence our assumption for average sinking velocity and the use of liner regression are
 562 proved to be reasonable.

563 **Appendix E. Statistical and error analyses**

564 The errors of measured separation ratio (R) and calculated sinking velocity (v) are mainly caused
 565 by counting coccolith, the error of which follows the Poisson distribution. To detect the influence of
 566 counting number on the result error, the error of separation ratio was simulated by 5000 times Monte
 567 Carlo calculations with assumptions that ' $V_1:V_2=15:10$ ' and ' $n_1=n_2$ ' (Figure E1). The result shows
 568 that the number of coccolith counted in the upper column draws more influence on the relative error
 569 ($|R-R_{95CL}|/R$). That means more coccolith in the upper suspension should be counted to make results
 570 more accurate. The slope of $R_{cal}-T$ was calculated by liner fitting with the intercept fixed on
 571 $V_1/(V_1+V_2)$. The input R_{cal} were generated from measured values considering the error of coccolith
 572 counting (by the Matlab function 'random'). The regressions of $R_{cal}-T$ were repeated by 5000 times
 573 regressions in the software Matlab (by the function 'lsqcurvefit') and the error of sinking velocity,
 574 v, was source from the distribution slope of $R_{cal}-T$ in Monte Carlo process.



575

576 **Figure E1.** The error distribution with different N_1 and N_2 (ranging from 1 to 1000) simulated 5000
 577 times by the Matlab with assumptions that the error distributions of N_1 and N_2 fellow Poisson
 578 distribution. The calculation of R follows equation 2-5, and here we assume numbers of FOV are equal
 579 ($n_1=n_2$). Counter lines mark values equal to 5, 10 and 20. (a) and (c) represent the lower 95%
 580 confidence level and (b) and (d) represent upper 95% confidence level. (a) and (b) the relative error of
 581 R and (c) and (d) represent the absolute error of R.